International Conference on Nuclear Data for Science and Technology 2007
DOI: 10.1051/ndata:07435

95 MeV neutron scattering on hydrogen, deuterium, carbon and oxygen

P. Mermod[1], J. Blomgren[1,a], C. Johansson[1], A. Öhrn[1], M. Österlund[1], S. Pomp[1], B. Bergenwall[2], J. Klug[1], L. Nilsson[1], N. Olsson[3], U. Tippawan[4], P. Nadel-Turonski[5], O. Jonsson[6], A. Prokofiev[6], P.-U. Renberg[6], Y. Maeda[7], H. Sakai[7], A. Tamii[7], K. Amos[8], and R. Crespo[9]

[1] Department of Neutron Research, Uppsala University, P.O. Box 525, 75120 Uppsala, Sweden
[2] Department of Nuclear and Particle physics, Uppsala University, Sweden
[3] Swedish Defence Research Agency, Stockholm, Sweden
[4] Fast Neutron Research Facility, Chiang Mai University, Thailand
[5] The George Washington University, Washington, DC, USA
[6] The Svedberg Laboratory, Uppsala University, Sweden
[7] Department of Physics, University of Tokyo, Japan
[8] School of Physics, University of Melbourne, Australia
[9] Departamento de Fisica, Instituto Superior Técnico, Lisboa, Portugal

Abstract. Three neutron-deuteron scattering experiments at 95 MeV have been performed recently at The Svedberg Laboratory in Uppsala. Subsets of the results of these experiments have been reported in two short articles, showing clear evidence for three-nucleon force effects. In this paper, we present further discussion of the results. We obtained excellent precision in the angular range of the nd cross section minimum. The data are in good agreement with Faddeev calculations using modern *NN* potentials and including 3*N* forces from a 2π-exchange model, while the calculations without 3*N* forces fail to describe the data. CHPT calculations at next-to-next-to-leading order represent an improvement compared to calculations with *NN* forces only, but still underestimate the data in the minimum region. In addition to neutron-deuteron scattering data, neutron-proton and ^{12}C(n,n) elastic scattering data have been measured for normalization purposes, and ^{16}O(n,n) data have been obtained for the first time at this energy. It was possible to extract ^{12}C(n,n') and ^{16}O(n,n') inelastic scattering cross sections to excited states below 12 MeV excitation energy. These data are shown to have a significant impact on the determination of nuclear recoil kerma coefficients.

1 Introduction

Nuclear properties and interactions can be understood ab initio from the basic knowledge of the nucleon-nucleon (*NN*) interaction. For this purpose, *NN* potentials, which are based on meson-exchange theories, have been developed: the most widely used ones are the Argonne AV18 potential [1], the CD-Bonn potential [2,3] and the Nijmegen potentials [4]. After proper adjustment of the free parameters, these models are able to describe very well a restricted pp and np data base below 350 MeV [5].

In three-nucleon (3*N*) systems, quantitative descriptions can be provided rigorously by using *NN* potentials in the Faddeev equations [6]. However, theoretical considerations indicate that the description of systems made of more than two nucleons is not complete if three-body forces are not taken into account: 3*N* forces can be represented by introducing a 3*N* potential in the Faddeev equations. As a first experimental evidence, the ^{3}H and ^{3}He binding energies can be reproduced model-independently taking 3*N* forces into account [7], while calculations using only *NN* interactions underestimate them by typically half an MeV [2]. The ^{4}He binding energy can also be described correctly with combined *NN* and 3*N* forces [8], indicating that the role of four-nucleon forces is not significant.

The ultimate goal of nuclear physics would be to have a single consistent theory that could describe both nucleon and nuclear properties and dynamics. Chiral symmetry breaking can be analyzed in terms of an effective field theory, chiral perturbation theory (CHPT). This model can be applied to describe consistently the interaction between pions and nucleons, as well as the pion-pion interaction. Calculations made within the CHPT framework at next-to-next-to-leading order implicitly include 3*N* forces [9,10]. Calculations at the next higher order were made recently [11,12], allowing for instance an excellent description of *NN* phase shifts.

Besides the ^{3}H and ^{3}He binding energies, a number of observables that may reveal the effects of 3*N* forces have been identified. We will concentrate our discussion to nucleon-deuteron scattering in the energy range 65–250 MeV. At these energies, significant 3*N*-force contributions are expected in the elastic scattering angular distribution [13, 14] as well as for various spin-transfer observables in elastic scattering [6] and observables in the break-up process in various kinematical configurations [15,16]. In particular, for elastic nucleon-deuteron scattering, Faddeev calculations including a 3*N* potential with parameters adjusted to the triton binding energy predict that 3*N* forces affect substancially the differential cross section in the minimum region of the angular distribution [13]. Around 100 MeV, this effect is of the order of 30% in the minimum region.

Thus, a robust way to investigate 3*N* forces is to measure the proton-deuteron (pd) and neutron-deuteron (nd) elastic scattering differential cross sections. Numerous pd elastic scattering experiments have been performed [18–26].

[a] Corresponding author, e-mail: jan.blomgren@tsl.uu.se

©2008 CEA, published by EDP Sciences

Article available at http://nd2007.edpsciences.org or http://dx.doi.org/10.1051/ndata:07435

A coulomb-free signal can be obtained by performing nd scattering experiments [27–31]. In general, for both pd and nd scattering, in the energy range 65–150 MeV the data show the expected effects of 3*N* forces in the cross section minimum, while at higher energies, the effects tend to be too large to be accounted for by present theories. This might be due to the lack of a full relativistic treatment in the calculations [32,33]. At 95 MeV, the energy of the present work, relativistic effects are not expected to contribute significantly.

In the context of the nd scattering experiments, we obtained elastic scattering angular distributions for carbon and oxygen at 95 MeV. Differential cross sections for neutron inelastic scattering on carbon and oxygen to excited states below 12 MeV excitation energy could also be extracted [34]. These data are relevant for medical treatment of tumors with fast neutrons as well as in dosimetry, since the human body contains significant amounts of carbon and oxygen. Recoil nuclei from elastic and inelastic scattering are expected to account for more than 10% of the cell damage, the rest being mainly due to neutron-proton (np) scattering and neutron-induced emission of light ions [35,36]. The oxygen data may also be relevant for future incineration of nuclear waste in subcritical reactors fed by a proton accelerator, where the nuclear fuel might be in oxide form.

2 Results for np and nd scattering

By detecting either the scattered neutron or the recoil proton/deuteron, we were able to cover the angular range from 15 to 160 degrees in the c.m. system. By using two different detector setups, MEDLEY [37] and SCANDAL [38] in various configurations, we could keep the systematic uncertainties under control. Additionally, by measuring the np scattering differential cross section and, in the case where scattered neutrons were detected, also elastic scattering in carbon (i.e., the ^{12}C(n,n) reaction), the systematic error due to uncertainties in the normalization factors was minimized.

The np data are shown in figure 1. The absolute scale was adjusted to the Rahm et al. data [39] (filled triangles) which were in turn normalized to the well-known total np cross section [40]. The excellent agreement with both previous data and calculations based on *NN* potentials allows us to validate the quality of the nd data since the np and nd differential cross sections were measured under essentially the same conditions. Besides, the np data give supplementary information about the np angular distribution at 95 MeV (for previous data, see, e.g., refs. [39,40]). In many experiments, neutron cross sections are measured relative to the np cross section [40], i.e., it is used as a cross section standard. Neutron-proton scattering plays an important role in nuclear physics, since it can be used to validate *NN* potentials and to derive a value of the absolute strength of the strong interaction. The extensive database of np differential cross sections is not always consistent and, not unrelated, there are still problems with the determination of a precise value of the πNN coupling constant [5,41,42].

The nd results at 95 MeV in the minimum region ($80° < \theta_{\mathrm{c.m.}} < 160°$) are shown in figure 2, and are compared with theoretical predictions based on Faddeev calculations [13] using the AV18 *NN* potential [1] combined with two different

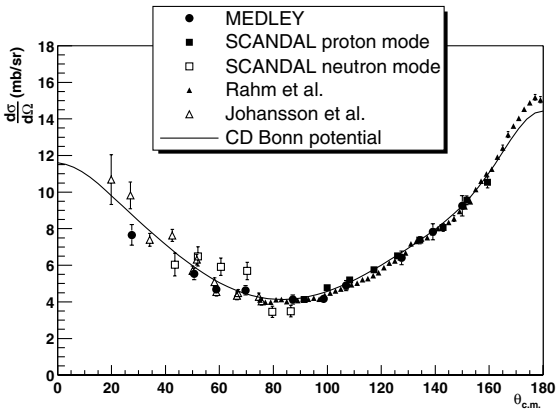

Fig. 1. The present and previous Uppsala data for np elastic scattering at 95 MeV. The dots and squares are the results of our nd experiments [28,29], and the triangles were obtained from previous np experiments by Rahm et al. [39] and Johansson et al. [40]. The data are compared with a calculation using the CD-Bonn *NN* potential [2].

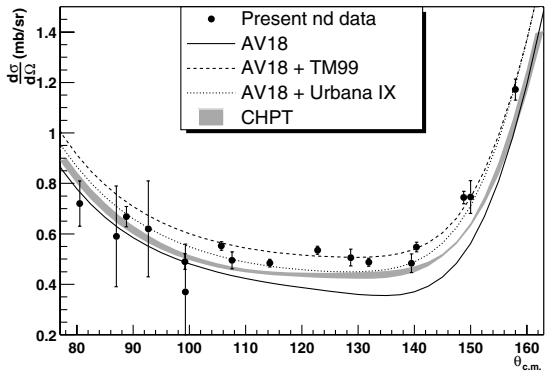

Fig. 2. The present nd data (filled dots) in the angular range $80° < \theta_{\mathrm{c.m.}} < 160°$. The solid, dashed, and dotted curves were obtained from Faddeev calculations with the Argonne AV18 potential [1] without 3*N* forces, with the Tucson-Melbourne (TM99) 3*N* potential [43], and with the Urbana IX 3*N* potential [44], respectively. The gray band was obtained from chiral perturbation theory at next-to-next-to-leading order [9].

3*N* potentials (Tucson-Melbourne [43] and Urbana IX [44]), as well as predictions from CHPT [9]. It is quantitatively illustrative to compute the reduced χ^2 between our data and the calculations for the nd differential cross section in the minimum, i.e., all data points shown in the figure. When no 3*N* forces are included, the χ^2 is larger than 18. The best description is given by the CD-Bonn potential (version 1996) with the TM99 3*N* force, with a χ^2 of 2.1. With the AV18 potential (shown in the figure), the nd differential cross section is slightly better described with the TM99 3*N* potential (χ^2 = 2.3) than with the Urbana IX potential (χ^2 = 3.5). The CHPT prediction gives a χ^2 of 6.5. Note that the deviations from one may be partly due to the normalization uncertainties in the data [29,34].

3 Results for ^{12}C(n,n) and ^{16}O(n,n) scattering

Differential cross sections for elastic and inelastic neutron scattering on carbon and oxygen must be well known for a

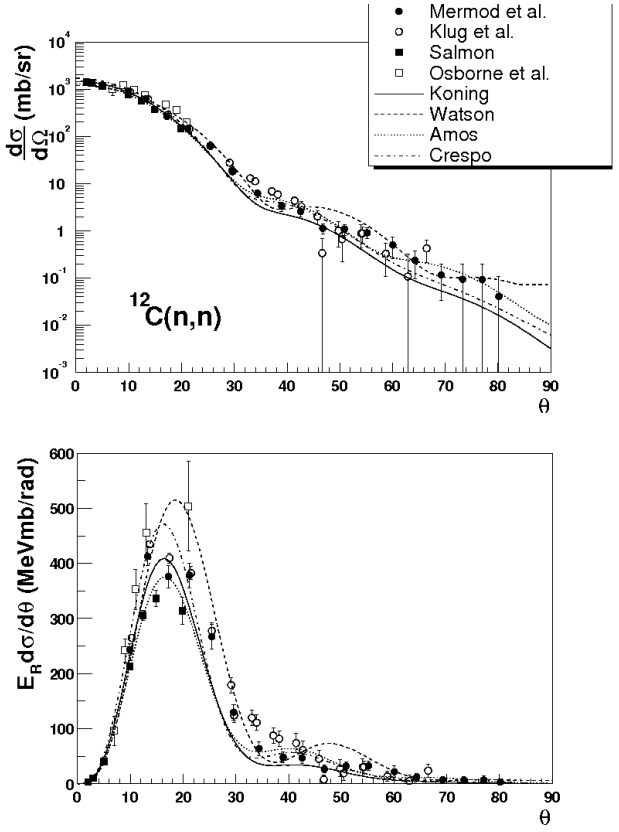

Fig. 3. Elastic neutron scattering on carbon at 96 MeV. The angle θ is the neutron scattering angle in the laboratory. The experimental data are from refs. [34,45–47]. The elastic scattering differential cross section is shown in the top panel, and in the bottom panel, the differential cross section was multiplied with the solid angle element and with the energy of the recoil nucleus. The area under this plot is proportional to the nuclear recoil kerma coefficient for elastic scattering.

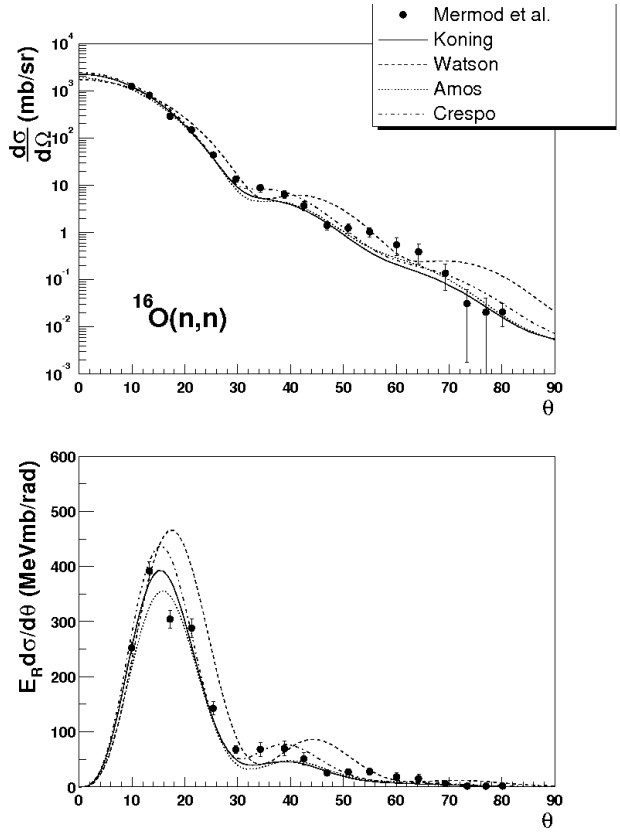

Fig. 4. Elastic neutron scattering on oxygen at 96 MeV. The angle θ is the neutron scattering angle in the laboratory. The experimental data are from ref. [34]. The elastic scattering differential cross section is shown in the top panel, and in the bottom panel, the differential cross section was multiplied with the solid angle element and with the energy of the recoil nucleus. The area under this plot is proportional to the nuclear recoil kerma coefficient for elastic scattering.

precise evaluation of the damage caused by fast neutrons in human tissue. Figures 3 (carbon) and 4 (oxygen) illustrate how recoil kerma coefficients are obtained from the differential cross sections. The elastic neutron scattering data at 96 MeV are from Mermod et al. [34], Klug et al. [45], Salmon [46] and Osborne et al. [47]. The theoretical curves are predictions from the Koning and Delaroche global potential [48], the Watson global potential [49], Amos et al. [50], and Crespo et al. [51] (see refs. [34,45] for details). In the top panels of the figures, the differential cross sections (in logarithmic scale) are plotted as functions of the neutron scattering angle in the laboratory. In the bottom panels, the distributions have been multiplied with the solid angle element $2\pi \sin\theta$ and weighed with the energy of the recoil nuclei E_R, thus illustrating the angular probability distributions for the neutrons to cause cell damage. As the solid angle vanishes at zero degrees, these distributions are no longer forward-peaked. Back-scattered neutrons transfer more energy to the nuclei than forward-scattered neutrons, and therefore the energy of the recoil nuclei increases with the neutron scattering angle. From these distributions, which peak at about 16°, we can deduce that, for elastic scattering, most of the damage is caused by neutrons scattered between 10 and 30°, but there is still a significant contribution up to 60°. With this way of plotting, the recoil kerma coefficient (and the cell damage due to elastic scattering) is proportional to the area under the distribution [34]. There are large variations among the different models, it leads to an uncertainty in the the recoil kerma coefficients of at least 10% for the theoretical calculations, while the experimental uncertainty reached with the present data is about 5%. For elastic scattering on carbon, most models are inaccurate in the region 25–35°. For oxygen, the prediction closest to the data is provided by the Koning and Delaroche potential. For inelastic scattering on carbon and oxygen at 96 MeV to collective states up to 12 MeV excitation energy, the main contribution to the kerma from inelastic scattering is between 30 and 60°. The data obtained in this angular range (not shown in the figures) tend to be significantly underestimated (by about 50%) by the calculations [34]. Although the contribution from inelastic scattering is small compared to other processes, the disagreement between calculations and data for inelastic scattering is still responsible for a significant (about 8%) discrepancy in the recoil kerma coefficient for the sum of elastic and inelastic reactions below 12 MeV excitation energy.

4 Conclusions

The np and nd elastic scattering differential cross sections at 95 MeV have been extensively and accurately measured. The data agree well with predictions based on *NN* and 3*N* potentials, provided that 3*N* forces are taken into account for nd scattering. This represents an important step to validate the approach in which *NN* and 3*N* potentials or effective field theories are used in ab initio models, which can be applied in systems of more than three nucleons.

As by-products of the nd experiments, elastic and inelastic neutron scattering differential cross sections on carbon and oxygen have been measured at 95 MeV. Experimental recoil kerma coefficients were obtained and shown to be quite sensitive to the differential cross sections in the angular range $25 - 70°$. This is relevant for the evaluation of deposited doses for applications such as dosimetry and fast neutron cancer therapy.

This work was supported by the Swedish Nuclear Fuel and Waste Management Company, the Swedish Nuclear Power Inspectorate, Ringhals AB, the Swedish Defence Research Agency and the Swedish Research Council.

References

1. R.B. Wiringa, V.G.J. Stoks, R. Schiavilla, Phys. Rev. C **51**, 38 (1995).
2. R. Machleidt, F. Sammarruca, Y. Song, Phys. Rev. C **53**, R1483 (1996).
3. R. Machleidt, Phys. Rev. C **63**, 024001 (2001).
4. V.G.J. Stoks, R.A.M. Klomp, C.P.F. Terheggen, J.J. de Swart, Phys. Rev. C **49**, 2950 (1994).
5. R. Machleidt, I. Slaus, J. Phys. G **27**, R69 (2001).
6. W. Glöckle, H. Witała, D. Hüber, H. Kamada, J. Golak, Phys. Rep. **274**, 107 (1996).
7. A. Nogga, A. Kievsky, H. Kamada, W. Glöckle, L.E. Marcucci, S. Rosati, M. Viviani, Phys. Rev. C **67**, 034004 (2003).
8. A. Nogga, H. Kamada, W. Glöckle, B.R. Barrett, Phys. Rev. C **65**, 054003 (2002).
9. E. Epelbaum, A. Nogga, W. Glöckle, H. Kamada, U.-G. Meissner, H. Witała, Phys. Rev. C **66**, 064001 (2002).
10. P.F. Bedaque, U. van Kolck, Annu. Rev. Nucl. Part. Sci. **52**, 339 (2002).
11. D.R. Entem, R. Machleidt, Phys. Rev. C **68**, 041001(R) (2003).
12. E. Epelbaum, W. Glöckle, U.-G. Meissner, Nucl Phys. **A747**, 362 (2005).
13. H. Witała, W. Glöckle, D. Hüber, J. Golak, H. Kamada, Phys. Rev. Lett. **81**, 1183 (1998).
14. S. Nemoto, K. Chmielewski, S. Oryu, P.U. Sauer, Phys. Rev. C **58**, 2599 (1998).
15. L.D. Knutson, Phys. Rev. Lett. **73**, 3062 (1994).
16. J. Kuroś-Żołnierczuk, H. Witała, J. Golak, H. Kamada, A. Nogga, R. Skibiński, W. Glöckle, Phys. Rev. C **66**, 024003 (2002).
17. S.A. Coon, M.D. Scadron, P.C. McNamee, B.R. Barrett, D.W.E. Blatt, B.H.J. McKellar, Nucl. Phys. **A317**, 242 (1979); S.A. Coon, W. Glöckle, Phys. Rev. C **23**, 1790 (1981).
18. O. Chamberlain, M.O. Stern, Phys. Rev. **94**, 666 (1954).
19. H. Postma, R. Wilson, Phys. Rev. **121**, 1229 (1961).
20. K. Kuroda, A. Michalowicz, M. Poulet, Nucl. Phys. **88**, 33 (1966).
21. G. Igo, J.C. Fong, S.L. Verbeck, M. Goitein, D.L. Hendrie, J.C. Carroll, B. McDonald, A. Stetz, M.C. Makino, Nucl. Phys. A **195**, 33 (1972).
22. R.E. Adelberger, C.N. Brown, Phys. Rev. D **5**, 2139 (1972).
23. H. Shimizu, K. Imai, N. Tamura, K. Nisimura, K. Hatanaka, T. Saito, Y. Koike, Y. Taniguchi, Nucl. Phys. A **382**, 242 (1982).
24. H. Sakai et al., Phys. Rev. Lett. **84**, 5288 (2000).
25. K. Hatanaka et al., Phys. Rev. C **66**, 044002 (2002).
26. K. Ermisch et al., Phys. Rev. C **68**, 051001(R) (2003).
27. H. Rühl et al., Nucl. Phys. A **524**, 377 (1991).
28. P. Mermod et al., Phys. Lett. B **597**, 243 (2004).
29. P. Mermod et al., Phys. Rev. C **72**, 061002(R) (2005).
30. J.N. Palmieri, Nucl. Phys. A **188**, 72 (1972).
31. Y. Maeda et al. (submitted to Phys. Rev. C).
32. H. Witała, J. Golak, W. Glöckle, H. Kamada, Phys. Rev. C **71**, 054001 (2005).
33. K. Sekiguchi et al., Phys. Rev. Lett. **95**, 162301 (2005).
34. P. Mermod et al., Phys. Rev. C **74**, 054002 (2006).
35. M.B. Chadwick, P.M. DeLuca Jr., R.C. Haight, Radiat. Prot. Dosim. **70**, 1 (1997).
36. J. Blomgren, N. Olsson, Radiat. Prot. Dosim. **103**, 293 (2003).
37. S. Dangtip et al., Nucl. Instrum. Meth. A **452**, 484 (2000).
38. J. Klug et al., Nucl. Instrum. Meth. A **489**, 282 (2002).
39. J. Rahm et al., Phys. Rev. C **63**, 044001 (2001).
40. C. Johansson et al., Phys. Rev. C **71**, 024002 (2005).
41. J. Blomgren, N. Olsson, J. Rahm, Phys. Scr. T **87**, 33 (2000).
42. M. Sarsour et al., Phys. Rev. Lett. **94**, 082303 (2005).
43. J.L. Friar, D. Hüber, U. van Kolck, Phys. Rev. C **59**, 53 (1999); S.A. Coon, H.K. Han, Few-Body Syst. **30**, 131 (2001).
44. B.S. Pudliner, V.R. Pandharipande, J. Carlson, S.C. Pieper, R.B. Wiringa, Phys. Rev. C **56**, 1720 (1997).
45. J. Klug et al., Phys. Rev. C **68**, 064605 (2003).
46. G.L. Salmon, Nucl. Phys. **21**, 14 (1960).
47. J.H. Osborne et al., Phys. Rev. C **70**, 054613 (2004).
48. A.J. Koning, J.P. Delaroche, Nucl. Phys. A **713**, 231 (2003).
49. B.A. Watson, P.P. Singh, R.E. Segel, Phys. Rev. **182**, 977 (1969).
50. K. Amos, P.J. Dortmans, H.V. von Geramb, S. Karataglidis, J. Raynal, Adv. Nucl. Phys. **25**, 275 (2000).
51. R. Crespo, R.C. Johnson, J.A. Tostevin, Phys. Rev. C **46**, 279 (1992).